# Supporting Information for:

# The Role of $Zn^{2+}$ Substitution on the Magnetic, Hyperthermic and Relaxometric Properties of Cobalt Ferrite Nanoparticles

Martin Albino,[a] Elvira Fantechi,[a,b] Claudia Innocenti,[a,c]* Alberto López-Ortega,[a,d] Valentina Bonanni,[a,e,§] Giulio Campo,[a] Francesco Pineider,[a,b] Massimo Gurioli,[f] Paolo Arosio,[e] Tomas Orlando,[g,†] Giovanni Bertoni,[h] Cesar de JuliánFernández,[h] Alessandro Lascialfari,[e] Claudio Sangregorio[c,a]*

[a] Department of Chemistry "U. Schiff", University of Florence and INSTM, 50019 Sesto Fiorentino (FI), Italy

[b] Department of Chemistry and Industrial Chemistry, University of Pisa and INSTM, 56124 Pisa, Italy

[c] C.N.R. – I.C.C.O.M. and INSTM, 50019 Sesto Fiorentino (FI), Italy

[d] Instituto de Nanociencia, Nanotecnología y Materiales Moleculares and Depto. de Física Aplicada, Universidad de Castilla-La Mancha, Campus de la Fábrica de Armas, 45071 Toledo, Spain

[e] Department of Physics, University of Milan, 20133 Milan, Italy

[f] Department of Physics and Astronomy, University of Florence, 50019 Sesto Fiorentino (FI), Italy

[g] Department of Physics and INSTM, University of Pavia, 27100 Pavia, Italy

[h] I.M.E.M- C.N.R Parco Area delle Scienze, 43124 Parma, Italy

[§] Present address: IOM-CNR, Basovizza, 34149 Trieste, Italy

[†] Present address: Max Planck Institute for Biophysical Chemistry, 37077 Göttingen, Germany

* claudia.innocenti@unifi.it; csangregorio@iccom.cnr.it

## §1. Synthesis of $Co_xZn_yFe_{3-x-y}O_4$

$Co_xZn_yFe_{3-(x+y)}O_4$ nanoparticles were prepared by thermal decomposition in high boiling solvent of metallic precursors in the presence of surfactants (oleic acid and oleylamine). The stoichiometry of the samples was controlled by adjusting the initial ratio of metal precursors in the synthesis. In order to keep the cobalt content constant ($x$ = 0.6) along the series, the ratio Co:Fe was fixed to 1:3.3 for all the samples prepared. On the other hand, the amount of Zn precursor was varied in order to obtain a series with increasing Zn-content up to $y$ = 0.40 (**Table S1**). Concerning this aspect, the amount of Zn effectively introduced into the spinel lattice (as measured by ICP-AES) was observed to be systematically lower than the amount set in the synthesis. It has already been observed in the literature that, using thermal decomposition technique the stoichiometry of the final product (in terms of relative metal concentration) often does not correspond to that of the initial mixture. This is mostly due to the different kinetics of decomposition of the various metal precursors (A. W. Orbaek *et al. J. Exp. Nanoscience* **2013**, 10, 5, 324–349, DOI: 10.1080/17458080.2013.832422). Therefore, in order to increase the effective Zn amount in the samples, an excess of Zn precursor was used. The excess was estimated by considering that a linear relationship between the final and starting Zn:Fe atomic ratio, was experimentally observed, as shown in **Figure S1**.

Moreover, in order to increase the size of the particles without affecting the composition, we found easier to replace the cobalt precursor or, alternatively, the zinc one, rather than modifying the other parameters of the synthesis.

**Table S1:** Initial molar amounts of metal precursors used in the synthesis

| Sample | mmol $Co(acac)_2$ 2 $H_2O$ | mmol $Fe(acac)_3$ | mmol $ZnCl_2$ |
|---|---|---|---|
| **CoFe00** | 0.198 | 0.66 | 0 |
| **CoZnFe05** | 0.198 | 0.66 | 0.088 |
| **CoZnFe13** | 0.198 | 0.66 | 0.132 |
| **CoZnFe27** | 0.198 | 0.66 | 0.558 |
| **CoZnFe40** | 0.198 | 0.66 | 0.873 |

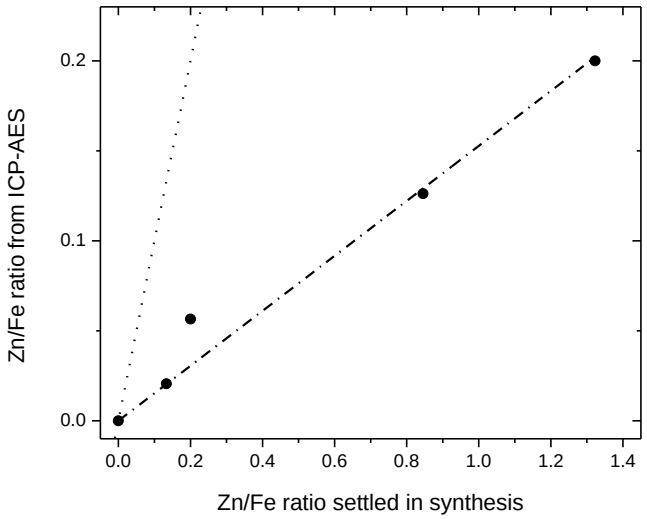


**Figure S1:** Relationship between initial Zn:Fe ratio and that found in the final product as evaluated by ICP-AES for the 8 nm series. The dashed line represents the fit of the data with a linear relationship, while the dotted line represents the 1:1 correspondence.

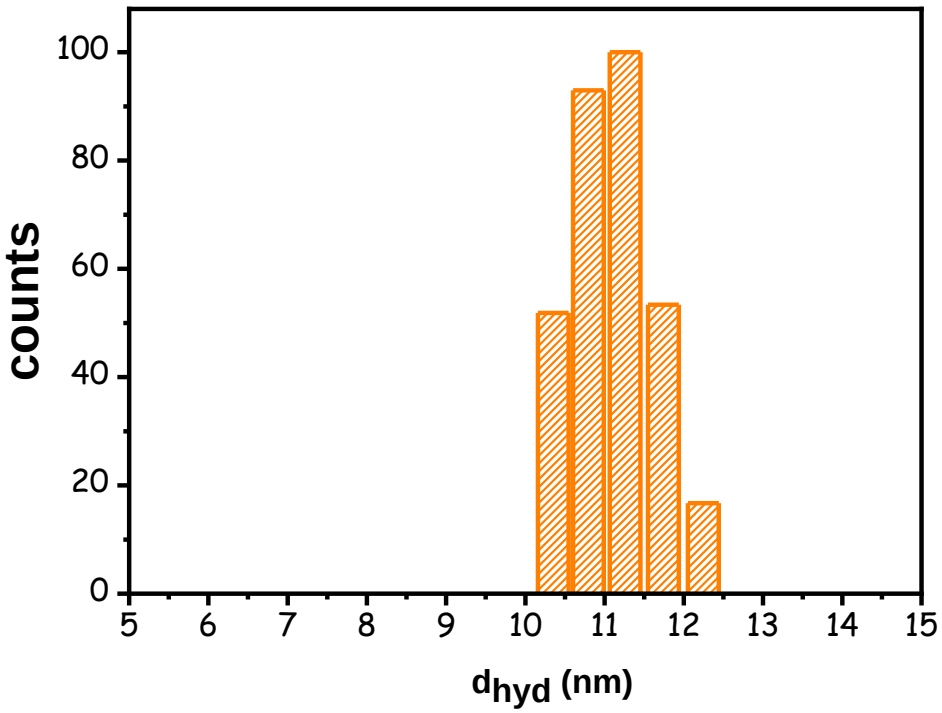


**Figure S2:** Representative measurement of hydrodynamic size, $d_{hyd}$, performed by dynamic light scattering technique on sample **CoFe00** in toluene**.** The average value is 11.1 nm with a standard deviation of 0.5 nm.

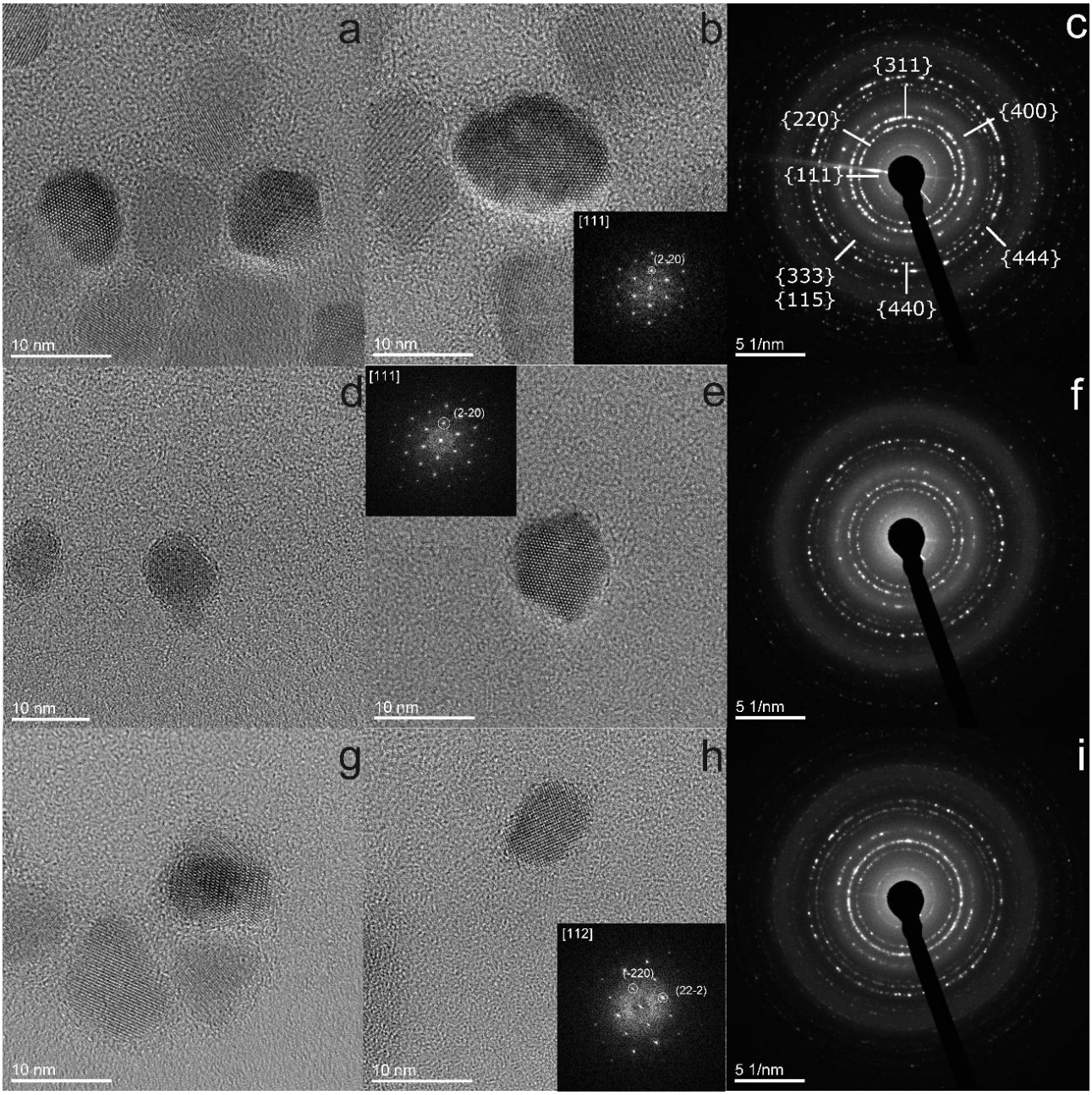


**Figure S3**. High-resolution images (a, b, d, e, g, h) and electron diffraction (c, f, i) of samples **CoZnFe13** (a, b, c), **CoZnFe27** (d, e, f) and **CoZnFe40** (g, h, i). In the inset of (b, e, h) the fast fourier transform (FFT) acquired on a single particle is reported.

## §2. Estimate of saturation magnetization

Spinels have general formula $AB_2O_4$, where A and B are divalent and trivalent metal ions, respectively. In the case of ferrites, the B ions are usually $Fe^{3+}$ and A are $Fe^{2+}$ or other divalent transition metal cations. Metal ions occupy part of the tetrahedral (*Td*) and octahedral (*Oh*) cavities generated by the arrangement of oxygen ions in a *fcc* structure. Depending on the distribution of metal ions among the different sites, ferrites are classified as normal or inverse spinels: in the first case, A and B ions occupy *Td* and *Oh* cavities, respectively; in the inverse structure, B ions are split between *Td* and *Oh* cavities while A ions occupy *Oh* sites.

The iron oxide magnetite ($Fe_3O_4$) has the structure of inverse spinel, $B(AB)O_4$. Considering only the spin contribution, the total magnetic moment of a single iron ion is 4 $\mu_B$ for $Fe^{2+}$ and 5 $\mu_B$ for high spin $Fe^{3+}$. In spinel ferrites the total magnetic moment arises from the antiferromagnetic coupling of the two ferromagnetically ordered tetrahedral and octahedral sublattices (**Figure S4a**), and therefore in magnetite the resulting net magnetic moment per formula unit, $\mu$, is 4 $\mu_B$. In non-stoichiometric cobalt ferrite of formula $Co_xFe_{1-x}Fe_2O_4$, the progressive substitution of $Fe^{2+}$ with $Co^{2+}$ leads to a small decrease of $\mu$ depending on the degree of cobalt substitution $x$. In fact, considering a complete inverted spinel structure with all the $Co^{2+}$ ions located in the octahedral sites and the same spin coupling scheme of magnetite (**Figure S4b**), the net magnetic moment for formula unit will be $(4-x)\mu_B$ which, for $x = 0.6$ corresponds to $\mu = 3.4\ \mu_B$. Following the same argumentation, a further decrease of the net magnetic moment would be expected in the case of $Co_xZn_yFe_{1-(x+y)}Fe_2O_4$, due to the diamagnetic nature of the $Zn^{2+}$ ion ($\mu_B = 0$). However, $Zn^{2+}$ ions have a strong affinity for *Td* sites and then their introduction in the spinel lattice causes the replacement of a $Fe^{3+}$ ions in *Td* cavity, and its migration in an *Oh* site (**Figure S4c**). This migration modifies the balancing of the magnetic moments, which is now given by the relation $\mu = 5\ (1+y) + 3x + 4\ (1-x-y) - 5\ (1-y) = (4-x+6y)\mu_B$.

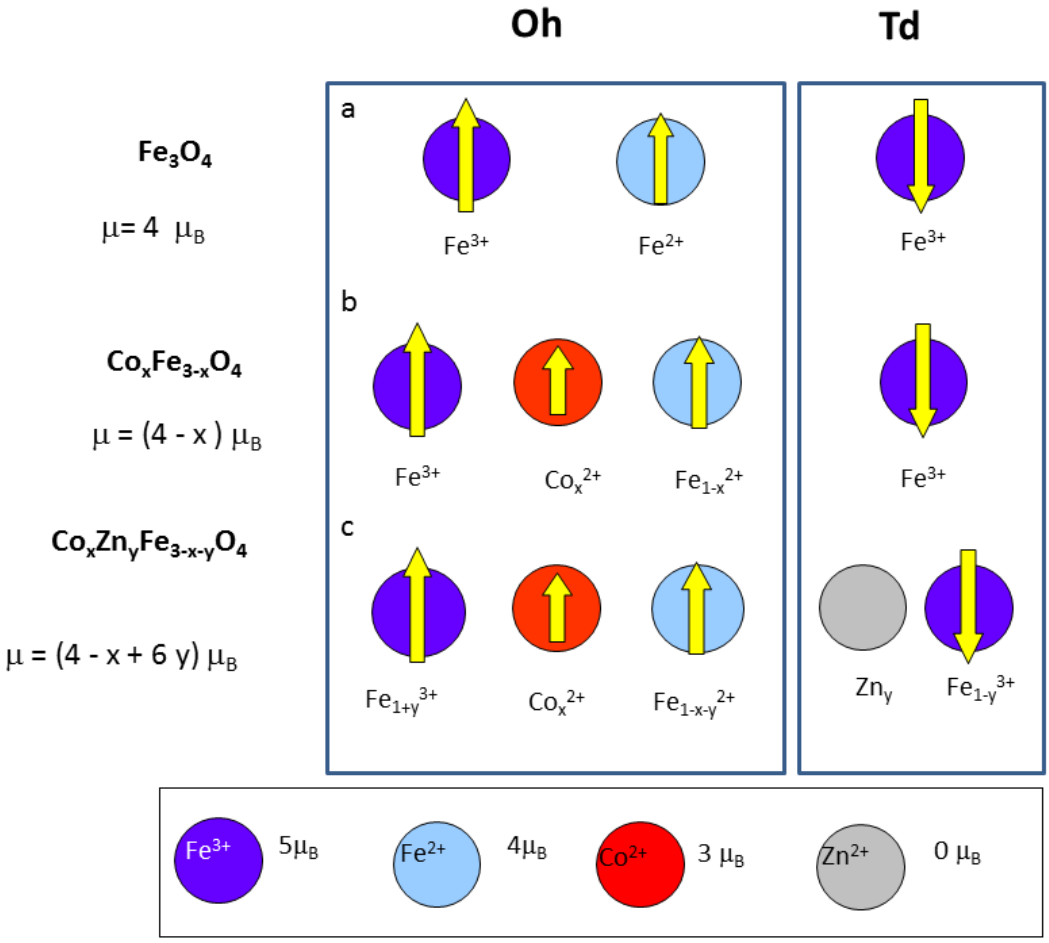


**Figure S4.** Scheme of the ion distribution between *Td* and *Oh* sites for: a) magnetite, b) cobalt ferrite, c) zinc doped cobalt ferrite. Colored circles denote different ions as reported in the bottom raw; the strength and direction of the ion magnetic moment is represented by the length and orientation of the superimposed arrow, respectively; $\mu$ is the net magnetic moment per formula unit and $\mu_B$ is the Bohr magneton ($9.274 \cdot 10^{-24}$ J/T).

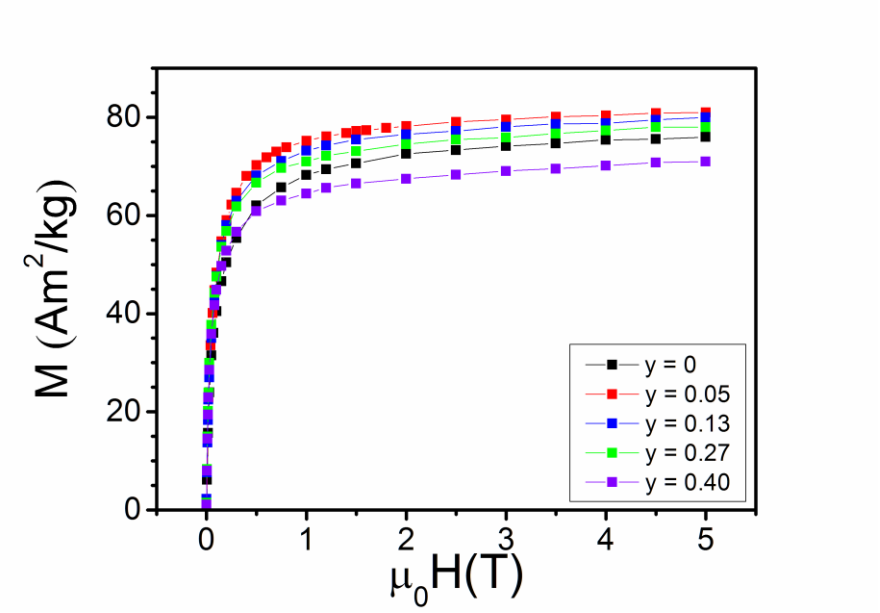


**Figure S5.** Magnetization curves, *M*(*H*), at room temperature (300K).

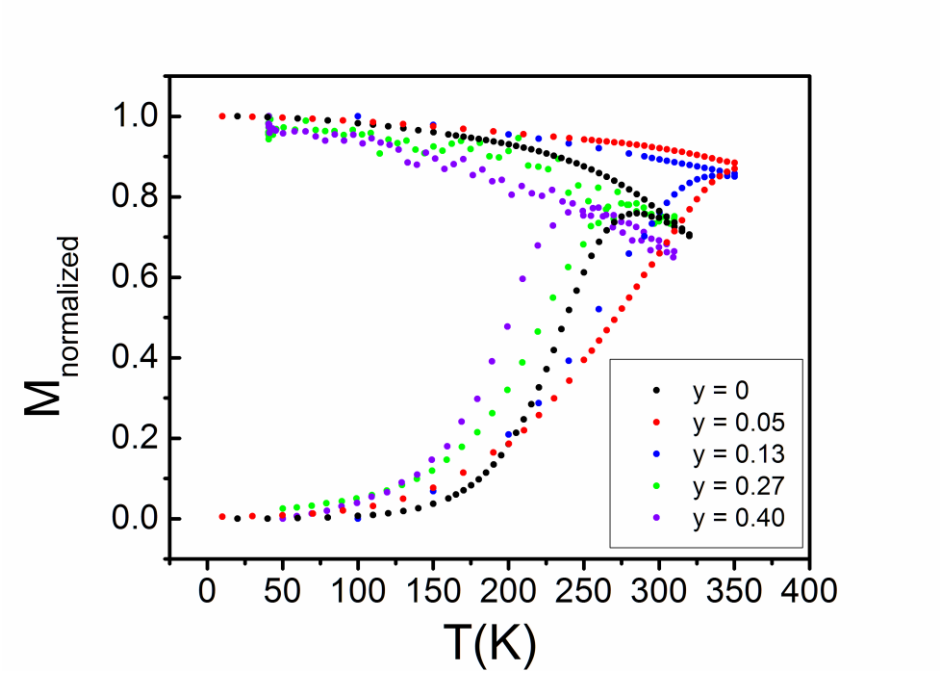


**Figure S6.** Temperature dependence of the zero field cooled (ZFC) and field cooled (FC) magnetizations for $Co_xZn_yFe_{(3-x-y)}O_4$ NPs, normalized to the maximum of the FC curve. All curves were acquired with a 5 mT probe field.

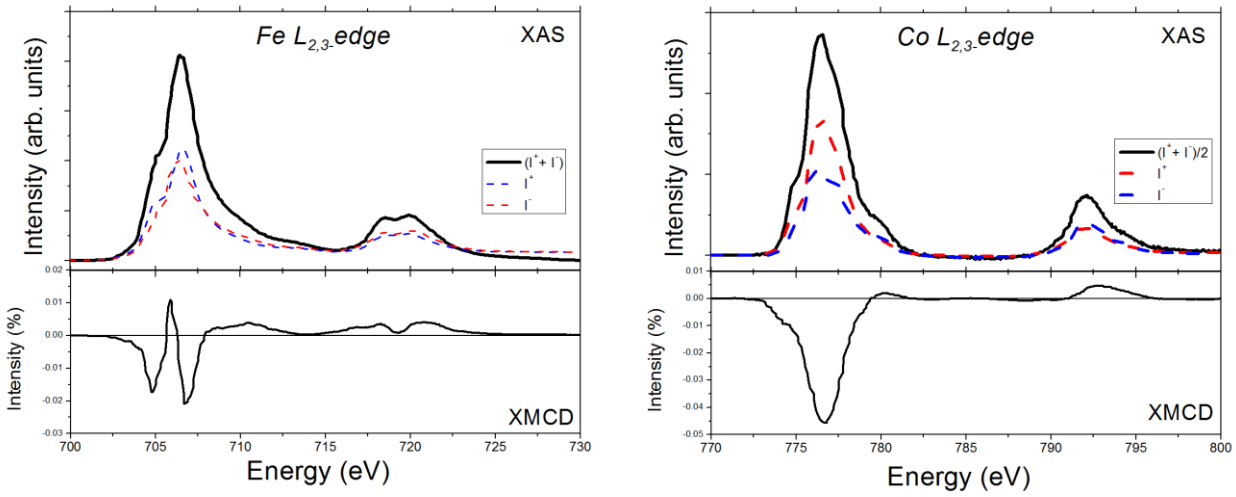


**Figure S7.** XAS and XMCD spectra at the Fe and Co $L_{2,3}$ edges for sample **CoFe00** as representative of the series. $I^+$ (blue dashed lines), $I^-$ (red dashed lines) and ($I^+$+$I^-$) (black lines) refers to right, left circularly polarized light and their sum, respectively.

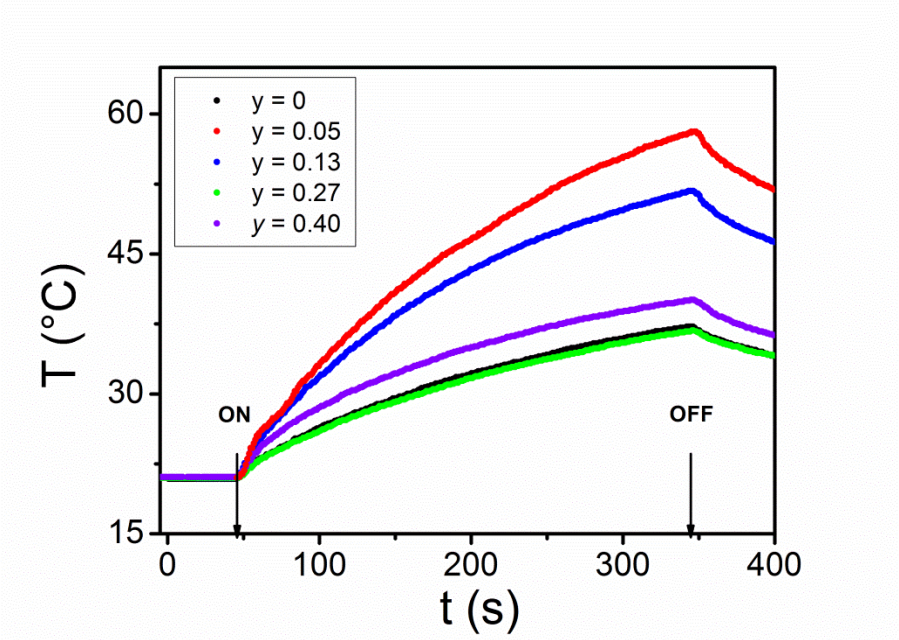


**Figure S8.** Temperature kinetic curves of $Co_xZn_yFe_{(3-x-y)}O_4$ NPs, acquired during the exposition to an alternate magnetic field ($H$ = 12 kA/m, 183 kHz). Arrows denotes the switching on/off of the external alternating field.

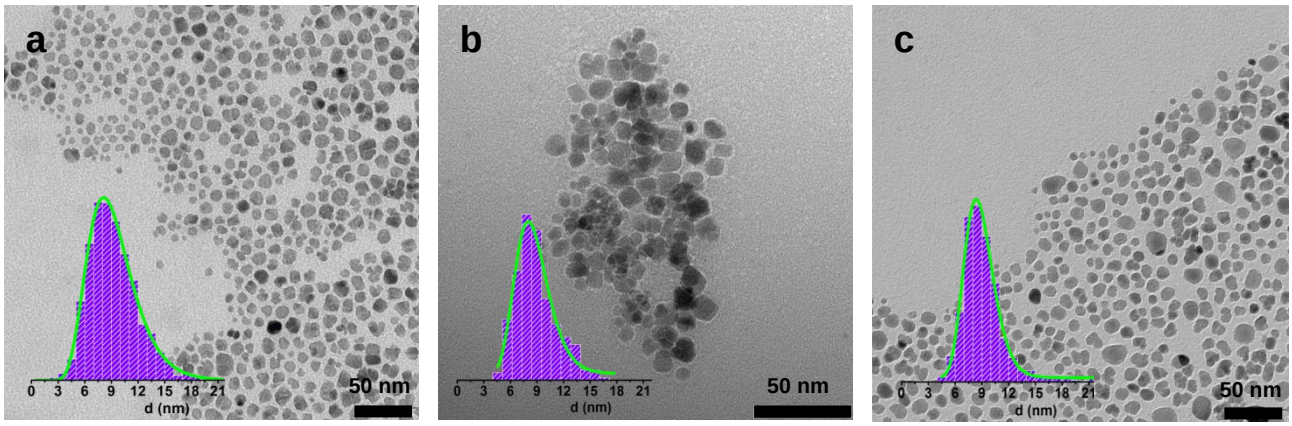


**Figure S9**. TEM images of $Co_xZn_yFe_{(3-x-y)}O_4$ NPs of 9 nm a) **CoFe05_9**, b) **CoZnFe11_9** and c) **CoZnFe26_9**. In the insets, the corresponding diameter distribution evaluated over 700-750 NPs is reported. The continuous line represents the best fit curve to a lognormal distribution.

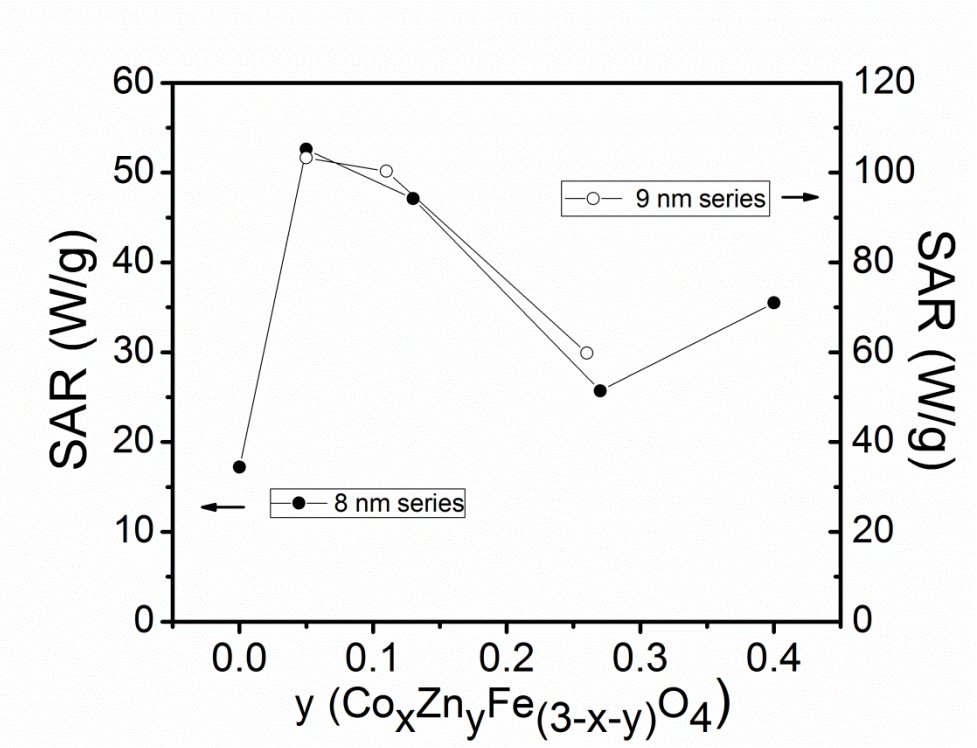


**Figure S10.** Comparison of experimental SAR values of **CoZnFeyy** and **CoZnFeyy_9** samples obtained at 183 kHz and 12 kA/m.

**Table S2.** Estimation of the atomic percentage of Cobalt, Zinc and Iron of $Co_xZn_yFe_{(3-x-y)}O_4$ NPs obtained by the EDS analysis (the error is estimated as 1%).

| | ***Fe atomic %*** | ***Zn atomic %*** | ***Co atomic %*** |
|---|---|---|---|
| **CoZnFe13** | 74.6 | 4.5 | 21.0 |
| **CoZnFe27** | 69.2 | 8.4 | 22.4 |
| **CoZnFe40** | 66.3 | 13.3 | 20.4 |

**Table S3.** Orbital, $\mu_{orb}$, and spin, $\mu_s$ components of the mean magnetic moment, $\mu_i$, of Fe and Co ions per formula unit, expressed in $\mu_B$, obtained from XMCD experiment.

| Sample | Fe ion | | | Co ion | | |
|---|---|---|---|---|---|---|
| | $\mu_{orb}$ | $\mu_s$ | $\mu$ | $\mu_{orb}$ | $\mu_s$ | $\mu$ |
| **CoFe00** | 0 | 4.0 | 4.0 | 0.47 | 2.9 | 3.4 |
| **CoZnFe05** | 0 | 3.6 | 3.6 | 0.35 | 2.1 | 2.7 |
| **CoZnFe27** | 0 | 3.6 | 3.6 | 0.36 | 2.3 | 2.4 |

**Table S4.** Chemical and structural properties of 9 nm $Co_xZn_yFe_{(3-x-y)}O_4$ NPs.

| Sample | $d_{TEM}$ (nm) | $d_{XRD}$ (nm) | $a$ (Å) | $x$ | $y$ | $z$ |
|---|---|---|---|---|---|---|
| **CoZnFe05_9** | 9.2 ±2.7 | 11.0 (6) | 8.404(1) | 0.46 | 0.05 | 2.46 |
| **CoZnFe11_9** | 9.0 ± 2.3 | 9.6 (5) | 8.415(1) | 0.55 | 0.11 | 2.30 |
| **CoZnFe26_9** | 9.2 ±2.4 | 10.1 (5) | 8.410(2) | 0.52 | 0.26 | 2.22 |

$d_{TEM}$: NP average diameter and standard deviation obtained from TEM analysis; $d_{XRD}$, $a$: crystallite mean size and lattice parameter obtained from XRD data analysis (errors on the least significant digit are reported in brackets); $x$, $y$, $z$: Co, Zn and Fe content obtained from ICP analysis.

**Table S5.** Magnetic and hyperthermic parameters of 9 nm $Co_xZn_yFe_{(3-x-y)}O_4$ NPs

| Sample | $\mu_{tot}$ | $T_B$ (K) | $M_{5T}$ at 5 K ($Am^2/kg$) | $M_{5T}$ at 300 K ($Am^2/kg$) | $\mu_0 H_C$ at 5 K (T) | $M_R$ at 5 K | $Ms$ calc. ($Am^2/kg$) | $SAR$ ($W/g_{Me}$) |
|---|---|---|---|---|---|---|---|---|
| **CoZnFe05_9** | 3.84 | >310 | 93 | 79 | 0.98 | 0.78 | 91.88 | 103.3± 1.3 |
| **CoZnFe11_9** | 4.11 | >310 | 91 | 74 | 0.93 | 0.75 | 97.99 | 100.3±1.8 |
| **CoZnFe26_9** | 5.04 | 280-290 | 103 | 82 | 0.55 | 0.65 | 119.48 | 59.8± 2.0 |

$\mu_{tot}$: average magnetic moment in $\mu_B$ units for chemical formula unit; $T_B$: blocking temperature; $M_{5T}$: experimental magnetization measured at 5T; $H_C$: coercive field; $M_R$: reduced remnant magnetization; $M_S$ calc.: theoretical value of saturation magnetization obtained as described in §1 of SI; $SAR$: SAR values per gram of metal (Co+Zn+Fe) obtained by applying an alternating magnetic field of 12 kA/m and 183 kHz.